Plasma-enhanced low temperature NH_3-SCR of NO_x over a Cu-Mn/SAPO-34 catalyst under oxygen-rich conditions

Boqiong Jiang[1], Shuang Zhao[1], Yaolin Wang[3], Yesheng Wenren[2], Zuchao Zhu[2], Jonathan Harding[3], Xinglin Zhang[4], Xin Tu[3*], Xuming Zhang[1, 2*]

[1]School of Environmental Science and Engineering, Zhejiang Gongshang University, Hangzhou 310018, China.

[2]State-Province Joint Engineering Lab of Fluid Transmission System Technology, Zhejiang Sci-Tech University, Hangzhou 310018, China

[3]Department of Electrical Engineering and Electronics, University of Liverpool, Liverpool L69 3GJ, UK

[4]Hefei General Machinery Research Institute Co. Ltd., Hefei 230031, China.

***Corresponding authors**

Miraclezhang918@163.com (X. Zhang); xin.tu@liverpool.ac.uk (X. Tu)

Abstract: In this work, a dielectric barrier discharge (DBD) plasma-enhanced NH_3-selective catalytic reduction (NH_3-SCR) of NO_x over a Cu-Mn/SAPO-34 catalyst at low temperatures (<200 ^oC) and oxygen-rich conditions (14 vol.%) has been investigated using a two-stage post-plasma-catalytic (PPC) configuration. The results show a maximum NO_x removal of 80% and a 100% N_2 selectivity without NH_3 slip or the formation of by-products at a low specific energy input (SEI) of 32 J/L. Adding water vapor (5.7 vol.%) into the plasma NH_3-SCR process does not negatively affect the removal of NO_x, while the presence of C_3H_6 enhances the removal of NO_x. *In situ* diffuse reflectance infrared spectroscopy (DRIFTS) combined with optical emission spectroscopic diagnostics has been employed to elucidate the reaction mechanism in the plasma-catalytic removal of NO_x. We find that the formation of NO_2 via NO oxidation in the first stage plasma gas-phase reaction enhances the Eley-Rideal (E-R) reaction on the surface of the Cu-Mn/SAPO-34 catalyst in the second stage catalytic NH_3-SCR of NO_x. The Cu-Mn/SAPO-34 catalyst shows stable performance in the plasma-enhanced NH_3-SCR of NOx after 5 cycles of catalyst regeneration. This work has successfully demonstrated a promising low-temperature plasma-catalytic solution for the effective NH_3-SCR of NO_x.

Keywords: Plasma catalysis; Cu-Mn/SAPO-34; Diesel exhaust gases; NH_3-Selective catalytic reduction; Reaction mechanism

1. Introduction

Nitrogen oxides (NO_x) emissions from diesel engines are regarded as one of the significant sources of air pollution [1]. Selective catalytic reduction (SCR) with NH_3 (NH_3-SCR) has been proven to be effective for the removal of NO_x. In this process, a diesel particulate filter (DPF) is placed upstream of the SCR unit to prevent the deposition of soot and ash on the catalyst. However, the presence of a DPF limits the reaction temperature (typically to below 200 ^oC) of the SCR process for the heavy-duty diesel engines operated during the cold-start period as well as for the light-duty diesel engines. This causes a fuel-penalty as the temperature required for NH_3-SCR of NO_x using commercial catalysts is at least 250 ^oC under oxygen-rich conditions [2][3]. Therefore, developing an NH_3-SCR process which can be operated at lower temperatures in the oxygen-rich exhaust is of great importance to achieve the fuel-economy targets [4].

Cu-zeolite catalysts have attracted considerable attention in the NH_3-SCR of NO_x under oxygen-rich conditions [5]-[7]. However, as shown in Table S1, the removal of NO_x using Cu-zeolite catalysts is typically low (<40%) at oxygen-rich (>5 vol.%), low temperatures (<200 ^oC) with a high NO/NO_x ratio (~1). Additionally, the presence of water vapor and hydrocarbons (HCs) in the exhaust gases could negatively affect the removal of NO_x. Ming et al. reported a NO_x removal of 80% using a Cu/SAPO-18 catalyst at 200-400 ^oC and the NO_x removal was not affected by either the hydrothermal treatment of the Cu/SAPO-18 catalyst or the presence of HCs [8]. Recently, we have demonstrated a NO_x removal of 90% using an Mn-doped Cu/SAPO-34 catalyst at 200 ^oC. At higher temperatures (250-450 ^oC), the removal of NO_x was

close to 100% with outstanding hydrothermal stability and HC resistance [9]. Nevertheless, this temperature window (250-450 ^{o}C) is still too high for the light-duty diesel engines as well as the heavy-duty diesel engines during their cold-start period.

Non-thermal plasma (NTP) has great potential to lower the temperature window of NH_3-SCR of NO_x below 200 ^{o}C. The most notable advantage of NTP technology is that NTP can generate energetic electrons and a range of chemically reactive species, all of which can induce various chemical reactions at low temperatures and ambient pressure [10][11]. Plasma-assisted NH_3-SCR of NO_x in an oxygen-rich atmosphere can be implemented using two configurations: single-stage in-plasma catalysis (IPC) and two-stage post-plasma catalysis (PPC) [12]-[14]. The single-stage IPC process has great potential to generate a synergetic effect directly from the plasma-catalyst interactions. Wang et al. found that placing a Cu-Mn/ZSM catalyst in a corona discharge led to complete conversion of NO_x at a high specific energy input (SEI) of 300 J/L [15]. Takahara et al. investigated the single-stage plasma-catalytic SCR of NO_x using a range of supported metal catalysts. Among the tested metals (Pt, Pd, Rh, Ag, Cu and Ni) and supports (SiC, Al_2O_3, SiO_2 and TiO_2), the Pt/Al_2O_3 catalyst exhibited the best performance (~40% NO_x removal and 30% N_2 selectivity) at 150 ^{o}C [16]. In the two-stage PPC process, the plasma catalysis synergy might be formed through interactions of the catalyst surface with reaction intermediates and/or long-lived reactive species produced in the first stage plasma gas-phase reactions [12]. Guan et al. investigated the NH_3-SCR of NO_x over a V_2O_5-WO_3/TiO_2 catalyst in a two-stage PPC process at below 200 ^{o}C (catalyst bed temperature) and an oxygen concentration of 6 vol.%. A NO_x removal of ~70% was achieved at an SEI of ~100 J/L and a

86 catalyst bed temperature of ~100 ^{o}C. However, without using the plasma, such a NO_x removal
87 (~70%) can only be obtained at a higher reaction temperature of 350 ^{o}C with a significant
88 formation of N_2O (> 20 ppm) [18]. Broer et al. found that the removal of NO_x was less than
89 50% in the two-stage plasma-assisted NH_3-SCR of NO_x using a V_2O_5-WO_3/TiO_2 catalyst at a
90 NO/NO_x ratio of 0.95 when the temperature of the catalyst bed was below 180 ^{o}C [19]. These
91 studies demonstrated the potential of using plasma catalysis for the denitrification of light
92 diesel exhaust. However, till now, only limited catalysts have been evaluated in the plasma-
93 assisted NH_3-SCR of NO_x. It is critical to design and develop more active and stable catalysts
94 to enhance the efficiency of this process further.

95 Plasma-catalysis is a complicated process, involving both plasma gas-phase reactions and
96 plasma-assisted surface reactions [20]-[22]. However, plasma-assisted surface reactions on the
97 catalyst surface are among the least understood phenomena in the hybrid plasma-catalytic
98 processes. It is crucial to get a better understanding of the reaction mechanism in the plasma-
99 catalytic SCR of NO_x to generate valuable knowledge to facilitate the rational catalyst design
100 and to optimize the reaction performance further. *In situ* diffuse reflectance infrared
101 spectroscopy (DRIFTS) has been widely used to probe surface reactions in conventional SCR
102 of NO_x. However, using *in situ* spectroscopy to elucidate the reaction mechanism in plasma-
103 catalytic chemical reactions, particularly the plasma-assisted NH_3-SCR of NO_x, is very limited
104 [23]-[26]. Using a single-stage IPC system, Stere et al. investigated the plasma-assisted HC-
105 SCR of NO_x using *in situ* DRIFTS, and they found that the mechanism of the HC-SCR reaction
106 in the presence of the plasma is similar to that using thermal activation [26]. Li et al. studied

107 the HC-SCR of NO over a Pt/Ba/Al_2O_3 catalyst in a two-stage PPC process. Their findings
108 showed that the formation of NO_2 via NO oxidation in the first stage plasma reaction
109 contributed to the enhanced NO removal in the post-plasma SCR reaction on the catalyst
110 surface [27]. However, the reaction mechanism on the catalyst surface in the plasma-assisted
111 NH_3-SCR of NO_x is far less understood and still mostly unclear.

112 Herein, two-stage plasma-enhanced low-temperature NH_3-SCR of NO_x over a Cu-
113 Mn/SAPO-34 catalyst has been investigated under the simulated exhaust conditions (i.e.
114 oxygen-rich and high NO/NO_x ratio) of light-duty diesel engines for the first time. A dielectric
115 barrier discharge (DBD) was used as an NTP source [28][29]. The combination of DBD with
116 the Cu-Mn/SAPO-34 catalyst in the two-stage PPC process further decreases the temperature
117 window of NH_3-SCR of NO_x. A post-plasma NH_3 injection was used to avoid the oxidation of
118 NH_3 by the plasma. The effect of SEI, C_3H_6 and water vapor on the plasma-assisted NH_3-SCR
119 of NO_x was investigated below 200 ^oC in terms of NO_x removal, N_2 selectivity and NH_3 slip.
120 The reaction mechanism in the two-stage plasma-assisted NH_3-SCR of NO_x has been proposed
121 and discussed by using a combined means of *in situ* DRIFTS and optical emission
122 spectroscopic (OES) diagnostics.

123

124 **2. Experimental**

125 **2.1 Experimental setup**

126 Figure 1a shows a schematic diagram of the experimental setup for NO reduction. A
127 stainless-steel mesh with a length of 45 mm was wrapped around a 370 mm-length quartz tube

(inner diameter 8.4 mm; wall thickness 1.3 mm) and served as the ground electrode for the DBD reactor. A stainless-steel rod with a diameter of 6 mm was placed in the quartz tube as a high voltage electrode. The discharge gap was fixed at 1.2 mm. A fixed-bed flow reactor was placed at the downstream of the DBD reactor, forming a typical PPC configuration. 2 mL catalyst was packed in the fixed-bed flow reactor at a gas hourly space velocity (GHSV) of 30,000 h^{-1}. The DBD reactor was connected to a high-voltage AC power supply (TH5-A, Yiya Electric Co.) and placed in an electric oven (T1000-D200, Xianke); thus, the temperature of the DBD reactor can be controlled to maintain the same temperature as the fixed-bed flow reactor.

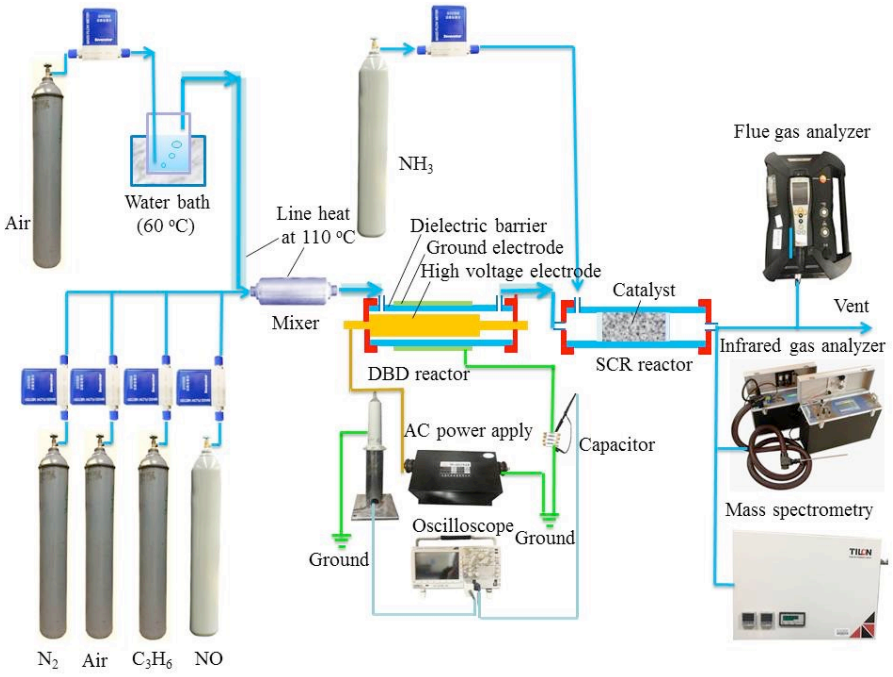

Figure 1. Schematic diagram of the experimental setup.

The simulated diesel engine exhaust included 300 ppm NO, 14 vol.% O_2, 0-5.7 vol.% H_2O, 0-300 ppm C_3H_6 and balanced N_2. To avoid the oxidation of NH_3 by NTP, post-plasma

142 injection of NH_3 (300 ppm) was performed in the SCR reaction. To control the concentration
143 of H_2O in the simulated gas mixture, a designated portion of air was passed through a bubbler
144 filled with distilled water and placed in a temperature-controlled water bath at 333 K. The total
145 gas flow rate was fixed at 1 L/min.

146 The electrical signals of the discharge were recorded using a digital oscilloscope (Tektronix
147 DPO3032). The discharge power was measured using the Q-U Lissajous method. The
148 concentration of NO, NO_2 and O_2 was measured using a flue gas analyzer (Testo 350, TESTO),
149 while the concentration of N_2O and N_2O_5 was determined by an infrared gas analyzer (PGD-
150 100, Madur E-commerce Co. Ltd., EU). The formation of gaseous products was also monitored
151 using mass spectrometry (LC-D200M, TILON). The concentration of NH_3 was monitored by
152 an NH_3 sensor (JC-NH_3, Jincheng Instruments). To understand the formation of nitrogen-
153 containing hydrocarbons, 5 ml aqueous dichloromethane (AR grade, Aladdin) was used to
154 adsorb the gaseous products for 1 h, followed by analysis using gas chromatography-mass
155 spectrometry (Agilent 7890A/5975C) equipped with an HP-5MS capillary column. The optical
156 emission spectroscopic diagnostics of the discharge was carried out using an emission
157 spectrometer (Acton SP-2500, Princeton Instruments) equipped with a highly sensitive camera
158 (PIXIS-100, Princeton Instruments) with a grating of 600 grooves/mm.

159 *In situ* DRIFTS was performed to understand the formation of adsorbed species on the Cu-
160 Mn/SAPO-34 catalyst surfaces in the post-plasma catalytic NH_3-SCR of NO_x using a Nicolet
161 is50 Fourier transform infrared (FTIR) spectrometer (Fig. S1). Before the experiment, the
162 catalyst powder (100 mg) was placed in a sample cell of the DRIFTS, and heated to 500 ^oC in

163 a 30 ml/min helium flow at a heating rate of 10 ^{o}C/min, held for 1 h, and then cooled to 140
164 ^{o}C. Two experimental modes were used in the *in situ* DRIFTS analysis to get new insights into
165 the surface reactions on the catalyst. In Mode I, the fresh catalyst was exposed to a gas mixture
166 when NTP was switched on (Mode I - plasma on) or off (Mode I - plasma off), and the adsorbed
167 surface species were investigated during the exposing period. In Mode II, two gas mixtures
168 were used; the fresh catalyst was pretreated with one gas mixture until the catalyst reached an
169 adsorption saturation, then the catalyst was exposed to the other gas mixture for investigating
170 the surface species. In the experiments (in Mode II), NTP could be switched on (Mode II -
171 plasma on) or off (Mode II - plasma off). Note that NH_3 was always injected into the system
172 after the plasma reactor and before the catalyst bed, known as post-plasma injection, in both
173 Modes I and II. The background spectrum was recorded before the catalyst was exposed to any
174 gas mixtures. The DRIFT spectra were collected in the range of 4000-650 cm^{-1} with a resolution
175 of 4 cm^{-1} in a Kubelka-Munk (K-M) format.
176
177 **2.2 Catalyst preparation and characterization**
178 Cu-Mn/SAPO-34 catalysts with different Cu/Mn molar ratios were prepared by a one-
179 pot hydrothermal synthesis method [9][30]. CuO (purity ≥ 99 %, Shanghai Lingfeng Chemical
180 Reagent Co. Ltd.) and MnO_2 (purity ≥ 85 %, Xilong Chemical Co. Ltd.) were used as the
181 precursor of Cu and Mn, respectively. To synthesize Cu-Mn/SAPO-34 (e.g. a Cu/Mn molar
182 ratio of 10:5), a crystallization solution was prepared with the following molar ratio of chemical
183 compounds in the solution: 0.07 CuO: 0.03 MnO_2: 0.1 SiO_2: 0.4 Al_2O_3: 2.0 H_3PO_4 (purity ≥

184 85 %): 0.02 HF (purity ≥ 40%): 1.0 C_3H_9NO: 83.3 H_2O. Firstly, CuO and MnO_2 were added
185 to the dilute solution of orthophosphoric acid, and the mixture was stirred at 80 ^oC until CuO
186 and MnO_2 were completely dissolved. The pseudo-boehmite (70% Al_2O_3) was then added at
187 room temperature to obtain a homogeneous gel under constant stirring. Subsequently, SiO_2,
188 morphinol and hydrofluoric acid were added to the gel and thoroughly stirred. A certain amount
189 of gel was then placed in a polytetrafluoroethylene (PTFE) bottle, sealed in a 50-ml autoclave
190 and kept at 190 ^oC for 3 days at autogenous pressure. The crystallized sample was washed with
191 distilled water and dried in air for 3 h before calcination in air at 600 ^oC for 5 h. The prepared
192 catalyst sample was pressed, crushed, and sieved to 60-100 mesh. Cu-Mn/SAPO-34 catalysts
193 with other Cu/Mn molar ratios were prepared in a similar way.

194 The effect of Cu/Mn molar ratio on the catalyst activity was evaluated, as shown in Fig.
195 S2. The optimal Cu/Mn molar ratio was found to be 10:5 at low temperatures (160 ^oC).
196 Therefore, this Cu/Mn molar ratio (10:5) was used in all the experiments in this study. The
197 regeneration of the catalyst was carried out at 500 ^oC and an air flow rate of 1 L/min.

198

199 The surface chemical states of the catalysts were examined by X-ray photoelectron
200 spectroscopy (XPS) with an Al Kα X-ray source (ESCALAB 250Xi, Thermo). The binding
201 energies of the spectra were calibrated using the C 1s level at 284.8 eV as an internal standard.
202 Concentrations of the elements were determined by the integration of peak areas in the XPS
203 data. The Brunauer-Emmett-Teller (BET) surface area of the catalysts was measured by N_2
204 adsorption-desorption isotherms at -196 °C using a physical adsorption instrument
205 (ASAP 2020-HD88, MicroMeritics). 100 mg of catalyst sample was pretreated at 150 ^oC for 6
206 h. The BET surface area of the catalysts was measured with a range of P_0/P from 10^{-9} to 1.0.

The morphologies of the fresh and spent Cu-Mn/SAPO-34 catalysts were analyzed using a scanning electron microscope (SEM, G2 pro, Phenom).

2.3 Calculation of parameters

The specific energy input was defined as:

$$\text{SEI (J/L)} = \frac{60 \times P}{Q} \quad (1)$$

Where P is the discharge power, and Q is the total gas flow rate.

The removal of NO_x ($NO + NO_2$) and N_2 selectivity were calculated using Eq. (2) and (3), respectively:

$$NO_x \text{ removal } (\%) = \frac{[NO_x]_{in} - [NO_x]_{out}}{[NO_x]_{in}} \times 100\% \quad (2)$$

$$N_2 \text{ selectivity } (\%) = \frac{[NO_x]_{in} - [NO_x]_{out} - 2[N_2O]_{out}}{[NO_x]_{in} - [NO_x]_{out}} \times 100\% \quad (3)$$

Where $[NO_x]_{in}$ and $[NO_x]_{out}$ are the inlet and outlet concentration of NO_x, respectively, and $[N_2O]_{out}$ was the outlet concentration of N_2O.

The maximum temperature changes due to the plasma heating effect (without extra heating) when varying the SEI can be estimated as follows:

228 $$\Delta T = \frac{60 \times P}{C \times m} \quad (4)$$

229

230 Where C is the averaged specific heat capacity of the reactants in J/kg·^{o}C and m is the total
231 mass flow of the reactants in kg/min.

232

233 **3. Results**

234 **3.1 Plasma-enhanced NH_3-SCR of NO_x**

235 Figure 2a shows the effect of SEI on the removal of NO_x and N_2 selectivity in the plasma
236 NH_3-SCR of NO_x at different reaction temperatures. Compared to the NH_3-SCR of NO_x
237 without using plasma (SEI = 0), the coupling of plasma with NH_3-SCR significantly enhanced
238 the NO_x removal, particularly at low temperatures (Fig. 2a). When the SEI increased from 0 to
239 27 J/L, the NO_x removal was increased from 9 to 50%, 40 to 72% and 66 to 80% at 100 ^{o}C,
240 140 ^{o}C and 180 ^{o}C, respectively. The effect of plasma on the removal of NO_x was more
241 significant at lower temperatures. In this study, the removal of NO_x is much higher than that
242 reported in previous studies under similar experimental conditions [7].

243 Figure 2a shows that the selectivity of N_2 is maintained at 100% and is almost independent
244 of the reaction temperature and SEI. Also, no residual NH_3, N_2O_5, N_2O or other by-products
245 (e.g., O_3) were detected in the exhaust gas (Table S2, Fig. S3 and Fig. S4), indicating that the
246 plasma-assisted NH_3-SCR of NO_x does not cause secondary pollution.

247

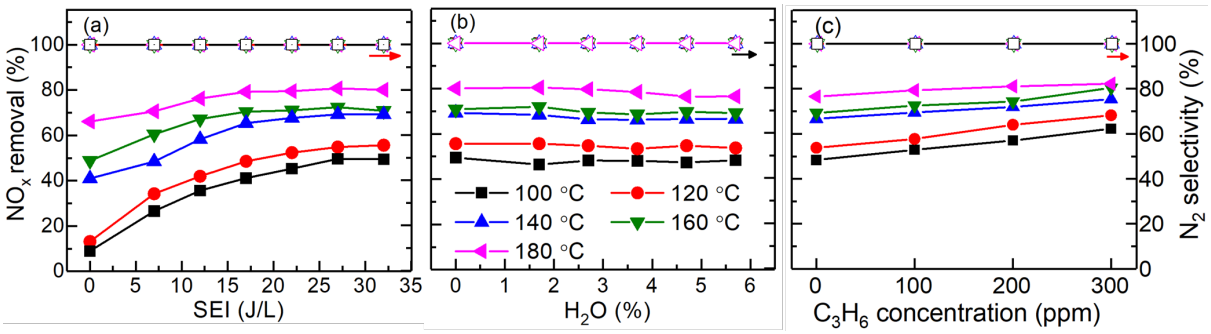

Figure 2. (a) Effect of SEI on NO_x removal and N_2 selectivity in the absence of water vapor and C_3H_6; (b) Effect of H_2O concentration on NO_x removal and N_2 selectivity in the absence of C_3H_6 at an SEI of 32 J/L; (c) Effect of C_3H_6 concentration on NO_x removal and N_2 selectivity in the presence of 5.7 vol.% H_2O at an SEI of 32 J/L. NO_x removal: closed symbols; N_2 selectivity: open symbols.

In conventional NH_3-SCR of NO_x, the presence of H_2O causes the competitive adsorption of H_2O, NO_x and NH_3 on the catalyst surface, leading to reduced efficiency of the NH_3-SCR reaction at low temperatures [31][32]. However, in the plasma-assisted NH_3-SCR of NO_x, we find that the presence of H_2O has a limited effect on the removal of NO_x and does not change the N_2 selectivity (100%), as shown in Fig. 2b.

Diesel engines generate large amounts of unburned hydrocarbons, such as C_3H_6 [33]. The dynamic diameter of C_3H_6 is relatively small (0.45 nm), thus it might bind to active sites of the catalyst and reduce the catalyst activity for the removal of NO_x in the conventional NH_3-SCR of NO_x [34][35]. Interestingly, in the plasma-assisted NH_3-SCR of NO_x, the presence of C_3H_6 in the plasma process enhanced the removal of NO_x (Fig. 2c). In addition, compared to the concentration of C_3H_6, the reaction temperature had a more significant effect on the removal

266 of NO_x in the plasma-assisted NH_3-SCR of NO_x with C_3H_6. At a C_3H_6 concentration of 300
267 ppm, the conversion of C_3H_6 increased from 66% to 83% when increasing the reaction
268 temperatures from 100 to 180 ^oC at an SEI of 32 J/L (Fig. S5). Higher C_3H_6 conversions can
269 be achieved at a lower initial concentration of C_3H_6 or a higher SEI. Previous works reported
270 that nitrogen-containing hydrocarbons might be produced in the plasma reduction of NO_x with
271 hydrocarbons [36][37]. In this work, only trace amounts of nitrogen-containing hydrocarbons
272 (mainly $C_{16}H_{31}NO$ and $C_{18}H_{35}NO$) were found with a total concentration of ~0.5 ppm (Fig.
273 S6).

274 In addition, the durability of the Cu-Mn/SAPO-34 catalyst in the plasma-assisted NH_3-
275 SCR of NO_x was evaluated at different reaction temperatures (100 - 180 °C). Figure 3a shows
276 a representative catalyst stability test at 180 °C and an SEI of 22 J/L. The Cu-Mn/SAPO-34
277 catalyst still maintained its good activity after 35 h time on stream at low temperatures and a
278 relatively low SEI. Although the removal of NO_x declined after 7 h, this value was still above
279 55% after 35 h reaction, which satisfies the China V emission standards [38].

280 It is important to note that the Cu-Mn/SAPO-34 catalyst shows an excellent regeneration
281 performance. Figure 3b shows that the removal of NO_x (initial removal efficiency) is almost
282 unchanged after 5 cycles of catalyst regeneration. In the catalyst regeneration experiments, the
283 removal of NO_x was quite stable with time on stream during each regeneration. In addition,
284 Fig. S7 shows that adding 20 ppm SO_2 (typical sulfur content in diesel) to this reaction has
285 limited effect on the NO_x removal, indicating the Cu-Mn/SAPO-34 catalyst is highly resistant
286 to SO_2.

The characterization of the fresh and regenerated catalysts (Fig. S8, S9, Table S3 and S4) was carried out. Table S3 shows the presence of Cu, O, Si, Al and P elements on the surface of the fresh and spent catalysts. In addition, compared to the fresh catalyst, the XPS analysis of the spent catalyst showed the presence of Mn and an enhanced concentration of Cu on the catalyst surface, suggesting that Cu and Mn could immigrate to the surface of the catalysts in the reaction. The XPS Cu2p spectra (Fig. S8) show Cu exists on the catalyst surface as Cu^{+} (932.6 ± 0.2 eV and 952.6 ± 0.2 eV), isolated Cu^{2+} in tetrahedrally coordinated sites (933.6 eV) and isolated Cu^{2+} in octahedrally coordinated sites (936.0 eV). After 5 cycles of catalyst regeneration, more Cu^{+} and octahedrally coordinated Cu^{2+} ions were detected on the surface of the spent catalyst (Table S4). Both Cu^{+} and octahedrally coordinated Cu^{2+} species have been proven to play an important role in the SCR reaction at low temperatures [39][40], which could contribute to the stable catalytic activity of the Cu-Mn/SAPO-34 catalyst. Moreover, Fig. S9 shows that the morphology of the catalyst does not change after 5 regenerations.

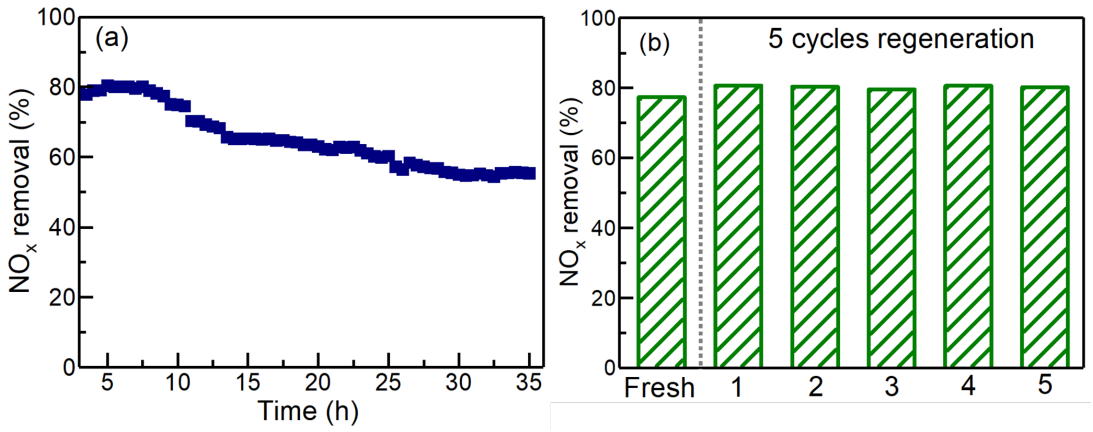

Figure 3. NO_x removal with the (a) reaction time, and (b) regenerated catalyst (5.7 vol.% H_2O + 300 ppm C_3H_6, SEI = 22 J/L and T = 180 ^{o}C).

3.2 Plasma conversion of NO_x without catalysts

Since the performance of NH_3-SCR of NO_x is strongly related to the concentration of NO_2 and the ratio of NO/NO_2 in the reaction [41], we measured the gas products in the first stage of the PPC process (i.e. after the plasma processing and before the NH_3-SCR of NO_x) to get a better understanding of the catalytic reactions on the surface of Cu-Mn/SAPO-34. Our preliminary study showed that the reaction temperature did not obviously affect the conversion of NO or the resulting products; thus, only the results at 140 ^oC are presented. As shown in Fig. 4a, increasing the SEI from 0 to 32 J/L reduced the concentration of NO from 267 to 192 ppm, but increased the concentration of produced NO_2 from 16 to 81 ppm. As a result, the NO_2/NO ratio increased from 0.06 to 0.42 when changing the SEI from 0 to 32 J/L. However, the total concentration of NO_x ($NO + NO_2$) slightly decreased from 282 to 272 ppm, indicating NO was mostly converted into NO_2 in the first stage plasma gas-phase reaction.

Compared to the plasma conversion of NO in the absence of H_2O, adding H_2O to the plasma reaction decreased the total concentration of NO_x ($NO + NO_2$), which can be attributed to the enhanced NO conversion and decreased NO_2 formation when adding H_2O (Fig. 4b). However, the presence of H_2O did not change the ratio of NO_2/NO (Fig. 4b).

Figure 4c shows the SEI has a considerable effect on the plasma conversion of NO in the presence of C_3H_6. More significant variations in the concentration of NO, NO_2 and NO_x, and the NO_2/NO ratio were observed when adding C_3H_6 into the reaction (Fig. 4c), indicating that C_3H_6 substantially affected the conversion of NO and the formation of NO_2.

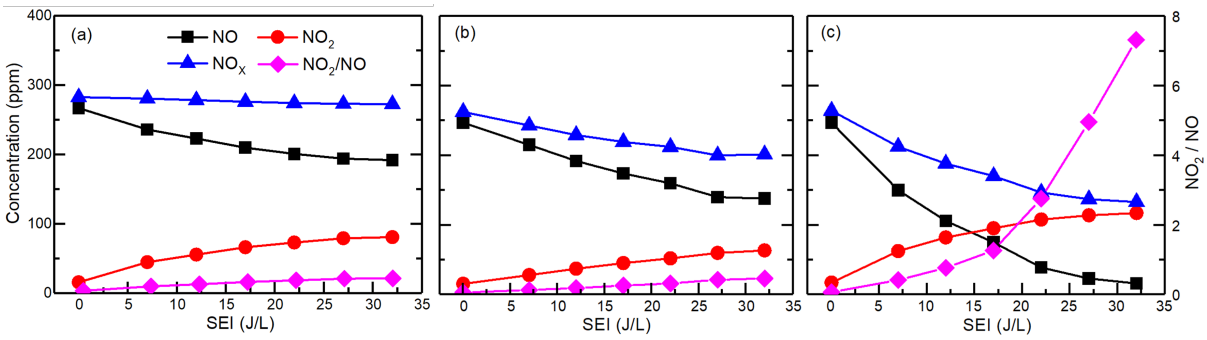

Figure 4. Effect of SEI on the concentrations of NO, NO_2 and NO_x, and NO_2/NO ratio in the gas products after the first stage plasma processing (at the outlet of the DBD reactor but before NH_3 injection) (a) 300 ppm NO; (b) 300 ppm NO + 5.7 vol.% H_2O; (c) 300 ppm NO + 5.7 vol.% H_2O + 300 ppm C_3H_6.

3.3 OES diagnostics

Emission spectra of the discharge were measured to better understand the formation of plasma generated reactive species in the first stage plasma processing of NO_x. Figure 5 shows the bands of N_2 and N_2^+ are dominant in the spectra of the discharge regardless of the gas composition as N_2 is used as a balance gas in this process. The atomic oxygen line can be detected in the spectra due to the production of O atoms via the dissociation of O_2 in the plasma. However, we cannot find OH molecular bands or H atomic lines in the spectra of the discharge with H_2O addition (Fig. 5b). Similarly, the spectrum of the discharge in the presence of C_3H_6 does not show any C_2 or CH molecular bands (Fig. 5c). It is worth noting that the absence of OH molecular bands does not mean that OH radicals are not produced in the plasma process in the presence of H_2O. Our previous work showed that over 97% of OH radicals are produced from the dissociation of H_2O by O atoms ($O + H_2O \rightarrow OH + OH$), while only <3% of OH

radicals are generated via electron impact dissociation of H_2O ($e + H_2O \rightarrow OH + H + e$) [42]. Thus, OH radicals are mostly produced in the ground state and are not observed in the spectra of the discharge.

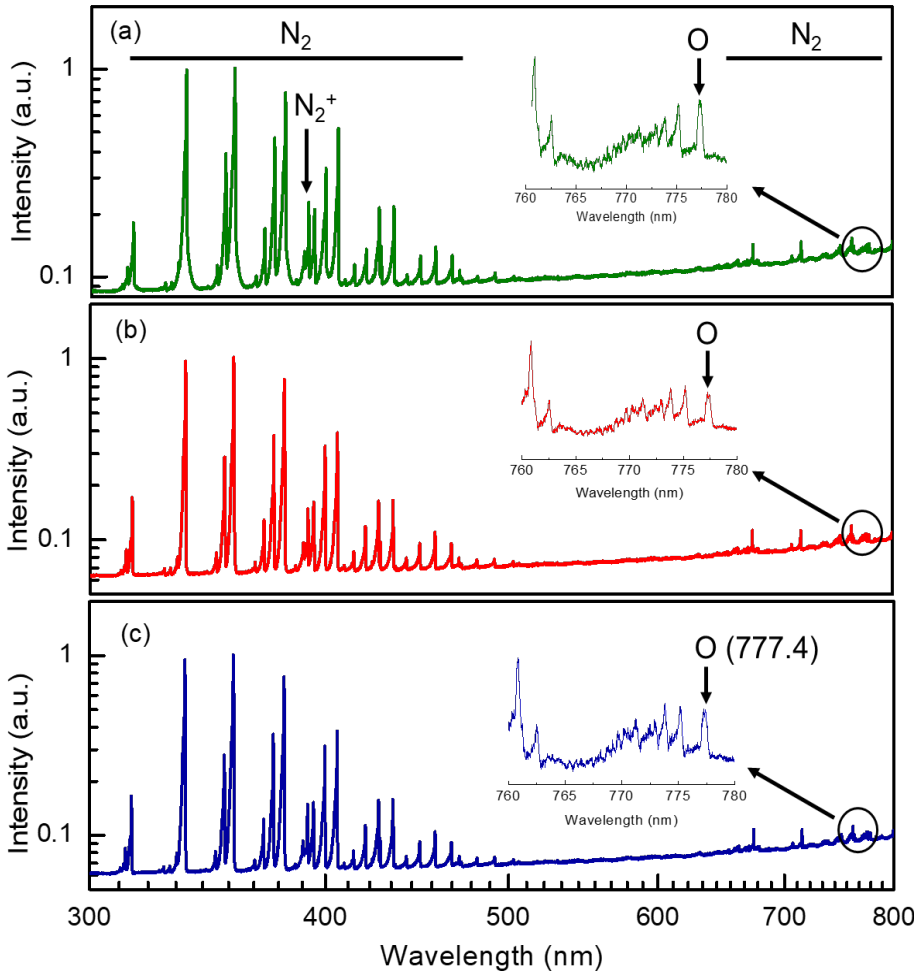

Figure 5. Emission spectra of DBD at (a) 300 ppm NO + 14 vol.% O_2; (b) 300 ppm NO + 14 vol.% O_2 + 5.7 vol.% H_2O; (c) 300 ppm NO + 14 vol.% O_2 + 5.7 vol.% H_2O + 300 ppm C_3H_6.

3.4 *In situ* DRIFTS analysis

The formation of intermediates on the catalyst surface in the post-plasma catalytic NH_3-SCR of NO_x was investigated using *in situ* DRIFTS. The DBD reactor used in this experiment was

the same as that used in the reaction. The Cu-Mn/SAPO-34 catalyst was placed after the DBD reactor in a typical PPC configuration. NH_3 was injected after the DBD reactor but before the catalyst bed, as shown in Figure S1. Helium was used as a carrier gas in the *in situ* DRIFTS experiment to increase the signal-to-noise ratio. The experimental mode I - plasma on was used in this section.

The *in situ* DRIFTS analysis of adsorbed species on the surface of Cu-Mn/SAPO-34 was carried out using different gas compositions in the PPC process. Figure 6a shows the IR spectra of adsorbed species on the catalyst surface using a flow of 300 ppm NO + 14 vol.% O_2. The band at ~1625 cm^{-1} can be assigned to the adsorbed NO_2 [43][44], while the bands at ~1605 and ~1300-1575 cm^{-1} are associated with the adsorption of monodentate nitrate and bidentate nitrate, respectively [45][46]. The intensity of these bands (adsorbed NO_2 and nitrates) increases with time and reaches the maximum at around 60 min.

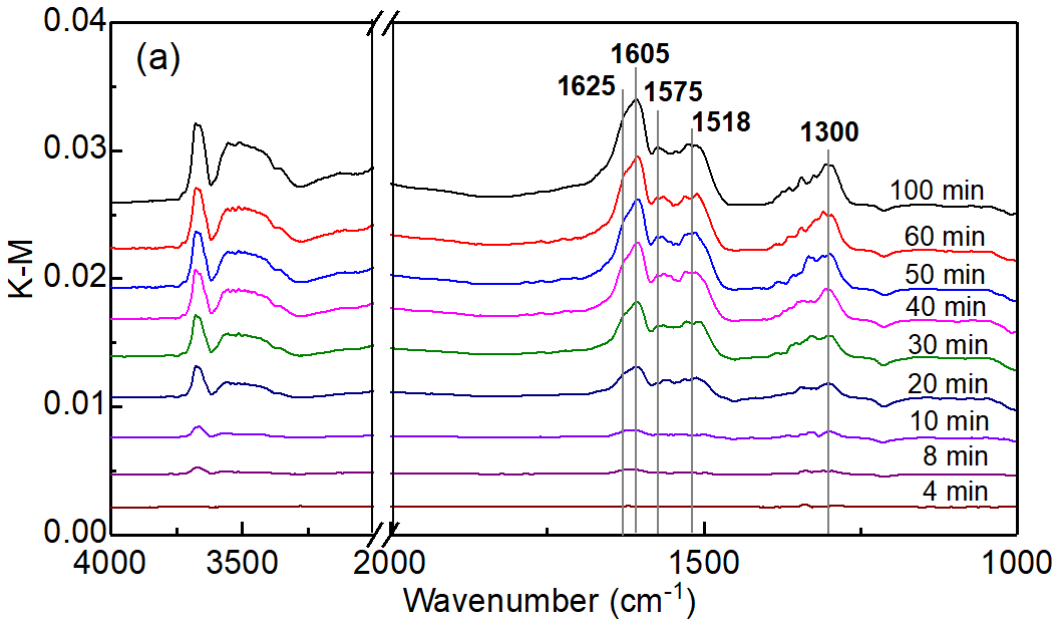

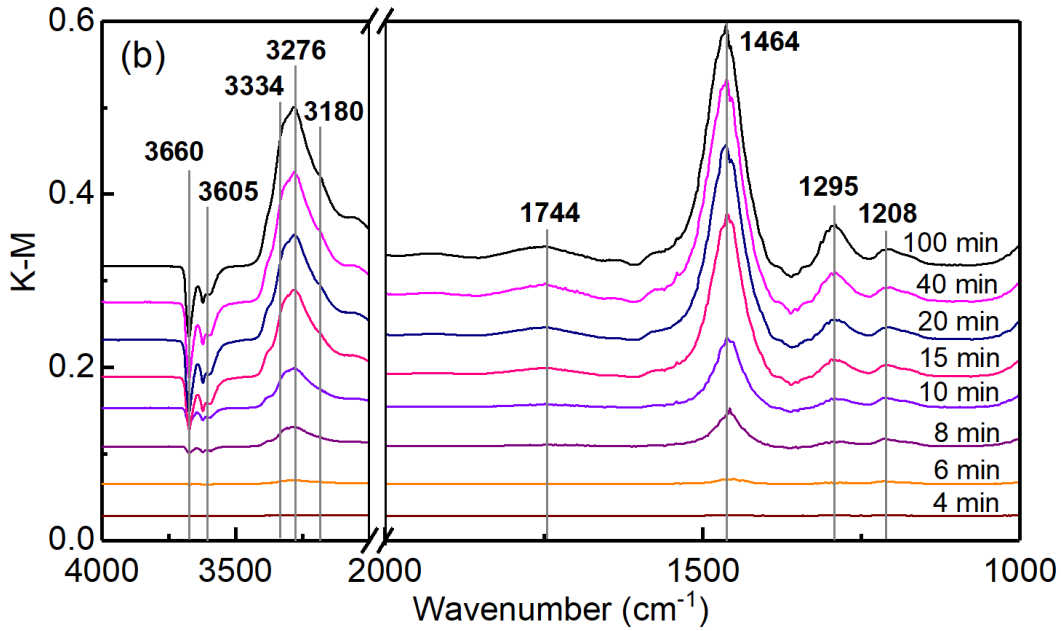
(b)
3660
3605
3334
3276
3180
1744
1464
1295
1208
100 min
40 min
20 min
15 min
10 min
8 min
6 min
4 min
K-M
Wavenumber (cm-1)

368

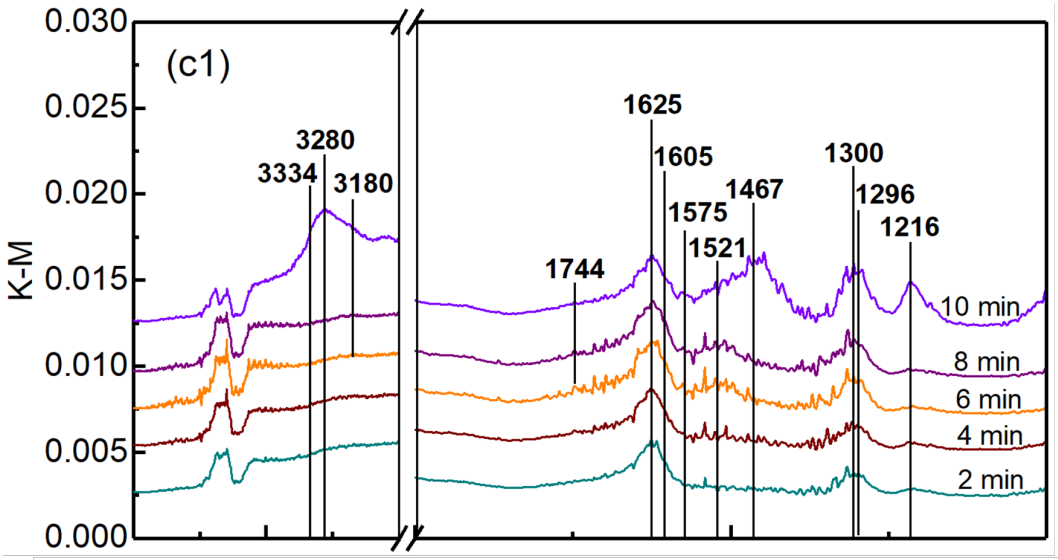
(c1)
3280
3334
3180
1744
1625
1605
1575
1521
1467
1300
1296
1216
10 min
8 min
6 min
4 min
2 min
K-M

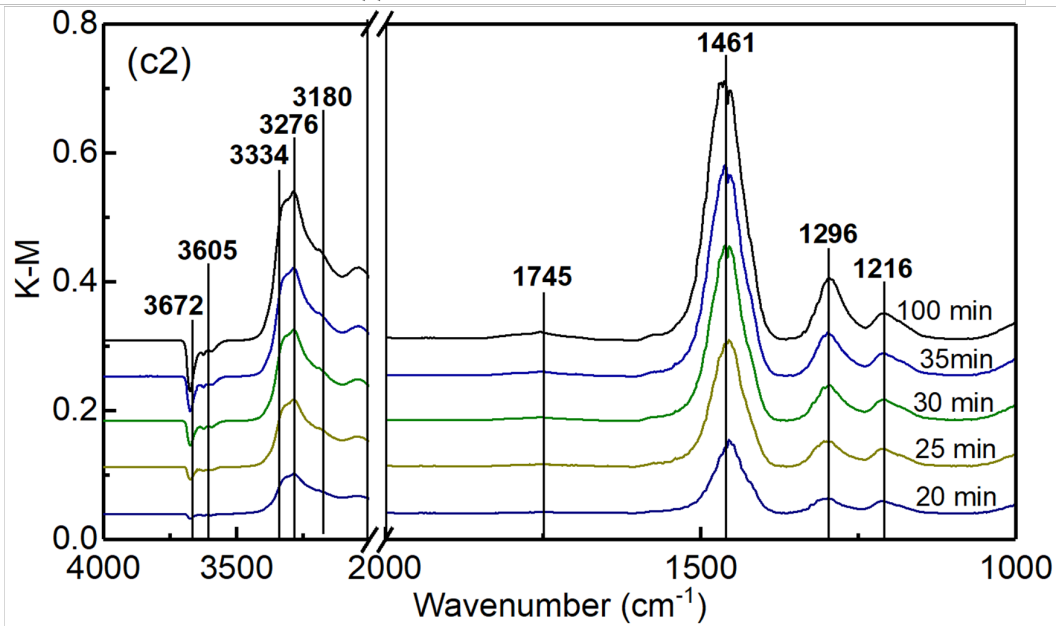
(c2)
3672
3605
3334
3276
3180
1745
1461
1296
1216
100 min
35min
30 min
25 min
20 min
K-M
Wavenumber (cm-1)

369

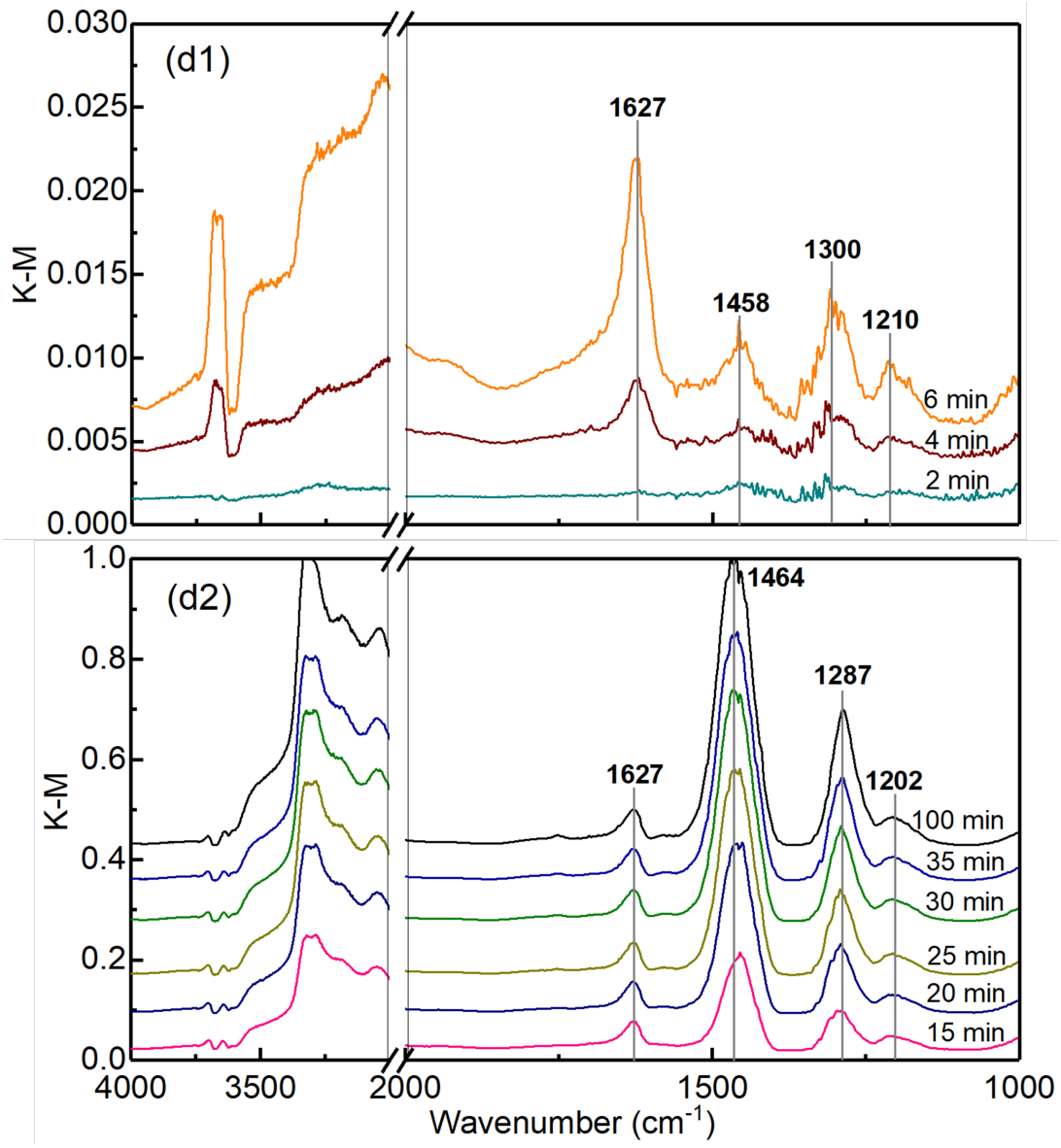

370

371

372

373

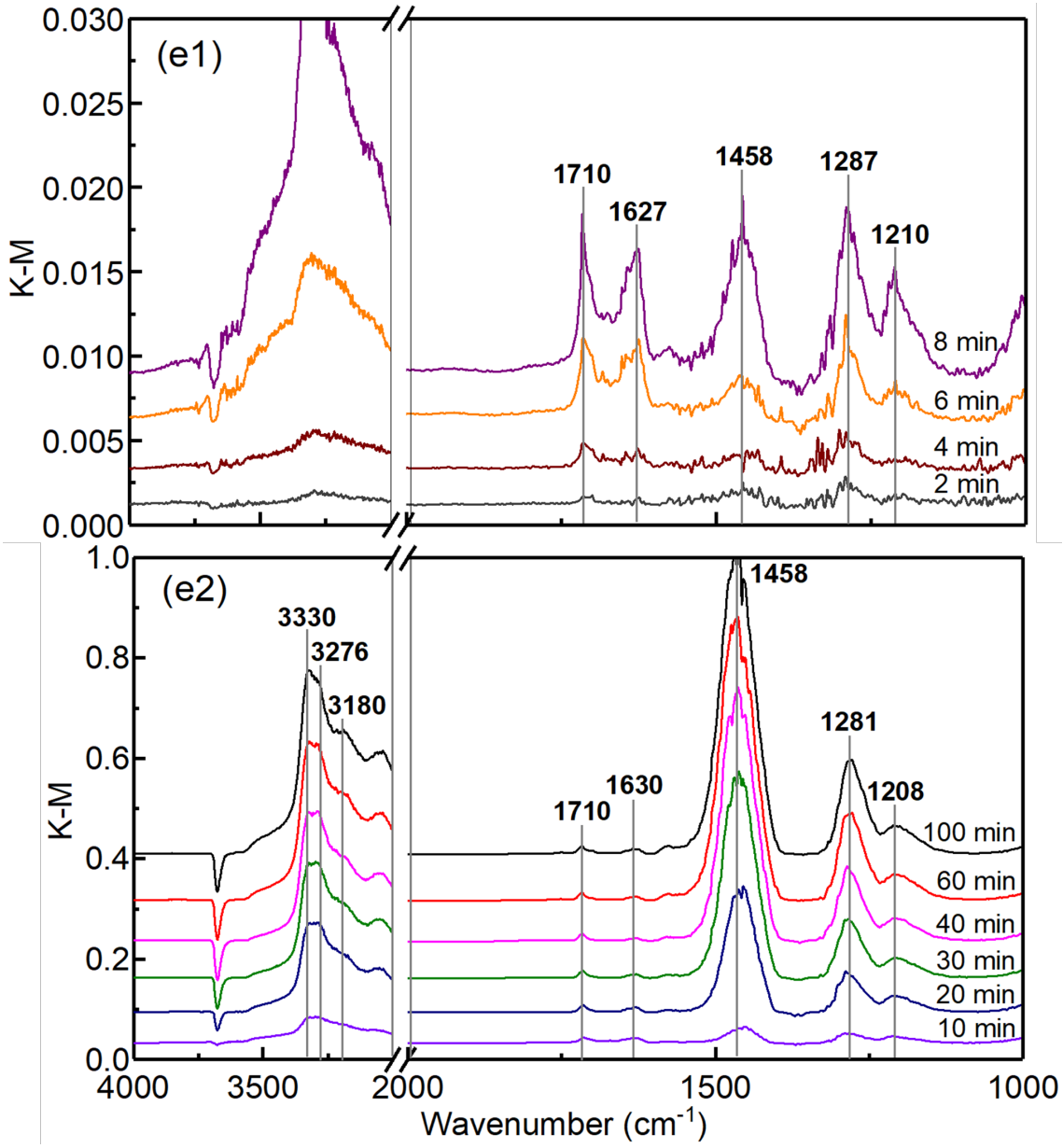

374

375 Figure 6. *In situ* DRIFTS spectra of adsorbed species on Cu-Mn/SAPO-34 using different gas

376 compositions (a) 300 ppm NO + 14 vol.% O_2; (b) 14 vol.% O_2 + 300 ppm NH_3; (c) 300 ppm

377 NO + 14 vol.% O_2 + 300 ppm NH_3; (d) 300 ppm NO + 5.7 vol.% H_2O + 14 vol.% O_2 + 300

378 ppm NH_3; (e) 300 ppm NO + 300 ppm C_3H_6 + 5.7 vol.% H_2O + 14 vol.% O_2 + 300 ppm NH_3

379 (Experimental mode I - Plasma, 140 ^oC).

380

Figure 6b presents the spectra of adsorbed species on the catalyst surface when using 14 vol.% O_2 + post-plasma injection of NH_3 (300 ppm). The bands at ~1467 and ~1745 cm^{-1} are associated with the adsorbed NH_4^+ species on Brønsted acid sites, while the bands at ~1210 and ~1295 cm^{-1} are related to the adsorption of NH_3 coordinated to Lewis acid sites [47][48]. In addition, the bands at 3267 and 3333 cm^{-1}, and 3180 cm^{-1} can be assigned to the adsorption of NH_4^+ and coordinated NH_3, respectively [49][50]. NO_x was not detected on the catalyst surface, indicating that the post-plasma injected NH_3 was not oxidized.

For the condition of 300 ppm NO + 14 vol.% O_2 + post-plasma injection of NH_3 (Fig. 6c1 and Fig. 6c2), the band of absorbed NO_2 appears at 2 min, and the intensity of this band increases with the time until 8 min and then decreases with time. The bands of NH_4^+ on Brønsted acid sites emerge at 10 min, later than the bands of NH_3 coordinated to the Lewis acid sites (appear at 2 min). However, the intensity of NH_4^+ increases more rapidly compared to that of the NH_3 coordinated to Lewis acid sites. In addition, we find that the bands (at 1521 and 1575 cm^{-1}) related to the adsorption of bidentate nitrate emerge (from 6 to 8 min) earlier than the bands of monodentate nitrate centered at 1605 cm^{-1} (at 10 min).

In Figure 6d, a He flow of 300 ppm NO + 5.7 vol.% H_2O + 14 vol.% O_2 passed through the DBD reactor and then mixed with the post-plasma injected NH_3 (300 ppm) before exposure to the catalyst. The band of absorbed NO_2 (1625 cm^{-1}) overlaps with that of H_2O. Before 8 min, the bands of NH_4^+ on Brønsted acid sites are weaker than that of the NH_3 coordinated to Lewis acid sites. After 8 min, the bands of NH_4^+ on Brønsted acid sites become stronger compared to the bands due to NH_3 coordinated to the Lewis acid sites. Compared to the IR spectra without

H_2O (Fig. 6c), we find the bands related to NH_4^+ on Brønsted acid sites and the NH_3 coordinated to Lewis acid sites show higher intensities.

Figure 6e shows the IR spectra of adsorbed species on the catalyst surface when using 300 ppm NO + 300 ppm C_3H_6 + 5.7 vol.% H_2O + 14 vol.% O_2 + post-plasma injection of NH_3 (300 ppm). The presence of the band at 1701 cm^{-1} indicates the formation of C=O groups on the catalyst [26][27]. The bands at ~1630 and 1290 cm^{-1} are associated with the presence of the C-C stretching vibration [26][27], and might cover the bands of adsorbed NO_2 and NH_3 coordinated to Lewis acid. The band at 1578 cm^{-1} that appears at 8 min could be related to the formation of carboxylate species or bidentate nitrate on the catalyst surface. The time-evolution of the bands (~1467 and 1210 cm^{-1}) associated with NH_3 is similar to that of the bands without C_3H_6 (Fig. 6d).

4. Discussion

4.1 Plasma-assisted NH_3-SCR of NO_x

In the two-stage post-plasma catalytic NH_3-SCR of NO_x, the contribution of the first stage plasma processing to the SCR of NO_x and enhanced NO_x conversion can be attributed to the following two effects: (1) enhancement of the SCR reaction due to the increased reaction temperature induced by NTP; (2) plasma generated intermediates promoting the SCR reaction on the catalyst surface. According to Eq. (4), if the plasma input energy is completely converted to heat, increasing the SEI of the plasma process from 0 to 27 J/L would enhance the catalyst temperature up to ~27 ^oC. Without using the NTP, the NO_x removal was only increased by ~5%

423 when increasing the catalyst temperature from 100 to 127 ^{o}C (Fig. S2). However, the removal
424 of NO_x using the PPC was enhanced by 41% (Fig. 2) when changing the SEI from 0 to 27 J/L
425 at a catalyst bed temperature of 100 ^{o}C. This result suggests that the plasma-induced heat effect
426 (temperature rise) has a neglectable impact on the enhanced NO_x removal, while the
427 intermediates generated in the first stage plasma process might significantly contribute to the
428 improved SCR of NO_x on the catalyst surface in the second stage of the process.

429 In the post-plasma catalytic NH_3-SCR of NO_x, NO can be oxidized by atomic O species
430 in the first stage plasma gas-phase reaction. The formation of atomic O species in the plasma
431 can be confirmed by the detection of O atomic lines in the OES diagnostics of the discharge
432 (Fig. 5), while the concentration of atomic O species increases with the increase of SEI [10].
433 As shown in Fig. 4a, the concentration of NO_2 increases rapidly with the rise in SEI at an SEI
434 of < 22 J/L. By contrast, at a higher SEI (> 22 J/L), the concentration of NO_2 increases slowly
435 with the SEI, which might be ascribed to the enhanced reverse reaction (Eq. 5) due to the
436 presence of a higher concentration of atomic O species [10].

437

438 $$NO_2 + O \rightarrow NO + O_2 \quad (5)$$

439

440 In thermal catalytic NH_3-SCR of NO_x on a Cu/SAPO-34 catalyst, we found that the
441 reduction of NO_x is mainly attributed to the reaction between adsorbed NO_2 and NH_4^+ via the
442 Langmuir-Hinshelwood (L-H) mechanism, and the reaction of gaseous NO with coordinated
443 NH_3 via the Eley-Rideal (E-R) mechanism [25]. The decomposition of bidentate nitrate

444 generates monodentate nitrate, followed by the formation of NO_2 via the conversion of
445 monodentate nitrate. In the post-plasma catalytic NH_3-SCR of NO_x, the amount of adsorbed
446 NO_2 with plasma on (Fig. 6a) was almost the same as that with plasma off (Fig. S10),
447 suggesting that the promotional effect of NTP is not through the L-H mechanism (e.g., the
448 reaction between adsorbed NO_2 and NH_4^+). The reaction between gaseous NO and NH_3
449 coordinated to Lewis acid sites is also not facilitated since the concentration of gaseous NO
450 decreased with plasma when compared to plasma off (Fig. 4), while the bands of coordinated
451 NH_3 with plasma on are the same as those with plasma off (Fig. 6b and Fig. S11).
452
453 It is worth noting that, in the IR spectra using 300 ppm NO + 14 vol.% O_2 (plasma on) with
454 300 ppm NH_3 post-plasma injection, we notice that the appearance of NH_4^+ band was delayed
455 (Fig. 6c1 and Fig 6c2), which might be ascribed to the reactions between adsorbed NH_4^+ and
456 NO_x complexes. To confirm which NO_x species reacts with NH_4^+, we measured the IR spectra
457 of the adsorbed species on the catalyst surface using 300 ppm NO + 14 vol.% O_2, followed by
458 14 vol.% O_2 + post-plasma injection of 300 ppm NH_3 with the experimental mode II. As shown
459 in Figure S12, the intensity of the adsorbed NO_2 band does not change from 4 to 15 min with
460 both plasma on and plasma off. Meanwhile, the intensities of the coordinated NH_3 bands in the
461 plasma on mode increase with time; however, the intensities of these bands are lower than
462 those with plasma off, and the bands of NH_4^+ are not observed in the plasma on mode. In the
463 plasma on mode, NO is converted to NO_2 only by NTP (Fig. 4a), and the amount of adsorbed
464 NO_2 does not change, suggesting that NO_2 formed in the gas-phase plasma is not further

adsorbed on the catalyst, it might be consumed through the reactions with the adsorbed NH_4^+ and coordinated NH_3 on the catalyst surface, offering an enhanced E-R reaction route contributing to the enhanced NO_x removal in the plasma-catalytic NH_3-SCR of NO_x.

4.2 Effect of H_2O

The presence of H_2O in the plasma reaction decreases the formation of NO_2 (Fig. 4b) but increases the intensities of the bands related to the adsorbed NH_4^+ and coordinated NH_3, suggesting that adding H_2O limits the consumption of NH_4^+ and coordinated NH_3 on the catalyst through the reactions with gaseous NO_2 (Fig. 6d1 and Fig. 6d2). To gain more evidence to support this hypothesis, we investigated the adsorbed species on the catalyst surface using 300 ppm NO + 5.7 vol.% H_2O + 14 vol.%O_2 followed by purging 5.7 vol.% H_2O + 14 vol.% O_2 with the post-plasma injection of 300 ppm NH_3 in experimental mode II, as shown in Fig. S13. Compared to the NTP reaction without H_2O, the NH_4^+ bands appear earlier, and the intensity of coordinated NH_3 bands increases when adding H_2O to the plasma reaction.

Our previous study also showed that the presence of H_2O limits the reaction of adsorbed NO_2 with NH_4^+ or coordinated NH_3, and thus decreases the efficiency of the NH_3-SCR of NO_x [51]. Although the reactions of gaseous and adsorbed NO_2 are inhibited, the presence of H_2O does not influence the efficiency of the plasma-assisted NH_3-SCR of NO_x (Fig. 2b). These findings indicate that there exists another reaction pathway for NO_x removal on the catalyst surface in the presence of H_2O. Previous studies reported that NH_3 could react with HNO_2 and HNO_3 initially formed on the catalyst surfaces to produce ammonium nitrites and ammonium

nitrates in thermal catalytic NH_3-SCR of NO_x over Fe- or Cu-based catalysts [52][53]. These nitrates and nitrites are unstable and can be easily decomposed on the catalyst surface, eventually generating N_2 and H_2O, as shown in Eq. (6) and (7).

$$HONO + NH_3 \leftrightarrow [NH_4NO_2] \rightarrow N_2 + 2H_2O \quad (6)$$

$$NH_3 + NO + \frac{1}{2}NH_4NO_3 \rightarrow \frac{3}{2}N_2 + \frac{5}{2}H_2O \quad (7)$$

In this study, the addition of H_2O decreases the concentration of NO and NO_2 at the exit of the DBD reactor (Fig. 4b), which suggests that HNO_2 and HNO_3 are formed via the reactions of water with NO and NO_2, as shown in Eq. (8) and (9) [28].

$$NO + OH \rightarrow HNO_2 \quad (8)$$

$$NO_2 + OH \rightarrow HNO_3 \quad (9)$$

Where OH could be produced from the reaction between O and H_2O as discussed in Section 3.

Plasma reduction of NO_x with NH_3 without a catalyst under the simulated exhaust conditions (i.e. oxygen-rich and a high NO/NO_x ratio) of light-duty diesel engines mainly produces NO_2 and ammonium salt with a negligible formation of N_2 [18][54]. In this study, we find the deposition of ammonium nitrites and ammonium nitrates in the SCR reactor if we remove the catalyst bed, changing the two-stage PPC configuration to a plasma only process. This finding further confirms that the presence of water in the NTP process forms ammonium nitrites and ammonium nitrates. However, when the catalyst is present (PPC configuration),

these species were not observed either in the SCR reactor or on the catalyst, indicating that they were further converted on the catalyst surface. Thus, adding water does not negatively affect the removal of NO_x as N_2 is the only N-containing gas product in the post-plasma catalytic SCR of NO_x.

4.3 Effect of C_3H_6

Previous studies reported that NO_2, HNO_x and N_2O are the major products in the plasma conversion of NO_x with C_3H_6 without a catalyst under the simulated exhaust conditions of light-duty diesel engines, while N_2 was not found in the gas products in these plasma-only processes [37][55]. In this study, the addition of C_3H_6 not only promotes the conversion of NO into NO_2 in the gas phase in the plasma stage (Fig. 4c), but also enhances the catalytic reduction of NO_x on the catalyst surface (Fig. 2c). In the first-stage plasma gas-phase reaction, the oxidation of C_3H_6 with O or OH radicals could generate oxygenates [56]. The following two effects might contribute to the enhanced reduction of NO_x: (1) the reaction of NO with oxygenates to produce N_2, as shown in Eq. (10); (2) the production of more gaseous NO_2 due to the consumption of O atoms by C_3H_6, limiting the reverse reaction (Eq. (5).

$$(8x - 4z + 2y)NO + 4C_xH_yO_z \rightarrow (4x - 2z + y)N_2 + 4xCO_2 + 2yH_2O \quad (10)$$

The increased formation of NO_2 in the plasma gas phase might enhance the reactions of $NO_2 + NH_4^+$, and NO_2 + coordinated NH_3 on the catalyst promoting the NO_x removal. The

528 presence of C_3H_6 delays the development of NH_4^+ and coordinated NH_3 on the catalyst surface
529 (Fig. 6e1 and Fig. 6e2), which could be attributed to the consumption of adsorbed NH_3 species
530 by gaseous NO_2 or the competing adsorption between C_3H_6 and NH_3. To clarify this, we
531 conducted the *in situ* DRIFTS analysis (experimental mode II- plasma on) using 300 ppm NO
532 + 300 ppm C_3H_6 + 5.7 vol.% H_2O + 14 vol.% O_2, followed by purging 5.7 vol.% H_2O + 14
533 vol.% O_2 with the post-plasma injection of 300 ppm NH_3. As shown in Fig. S14, the bands of
534 NH_4^+ (~1458 cm^{-1}) and coordinated NH_3 (1210 cm^{-1}) appear simultaneously at around 40 min,
535 which is much later than those in the reaction without C_3H_6 (20 min, Fig. S13). In addition, the
536 appearance of the bands of $NH_4^+$and coordinated NH_3 do not decrease the band intensities of
537 C-containing groups (1701 cm^{-1}, 1290 cm^{-1} and 1592 cm^{-1}), indicating the late appearance of
538 these bands ($NH_4^+$and coordinated NH_3) when adding C_3H_6 is not induced by the competing
539 adsorption between C_3H_6 and NH_3 on the catalyst surface. Considering the enhanced
540 concentration of gaseous NO_2 due to the addition of C_3H_6 (Fig. 4c), we propose that the higher
541 the concentration of gaseous NO_2, the later the appearance of the bands of NH_4^+ and
542 coordinated NH_3. In addition, previous studies proposed that the reaction between $C_xH_yO_z$ and
543 NO on the catalyst can also produce N_2 [57][58], where $C_xH_yO_z$ was produced in the gas phase
544 because catalyst could not oxidize C_3H_6 as confirmed by the IR spectra of the adsorbed species
545 on the catalyst surface when using 300 ppm C_3H_6 + 5.7 vol.% H_2O + 14 vol.% O_2 regardless
546 of the presence or absence of NO with experimental mode I- plasma off (Fig. S15). In this
547 study, the reaction between NO and $C_xH_yO_z$ over the catalyst was confirmed by the DRIFTS

548 spectra of the catalyst, which shows that the band intensities of oxygenates (e.g. 1592 cm^{-1})
549 decrease when NO is fed into the system, as shown in Fig. S14.
550
551 **4.4 Reaction pathways in the plasma-enhanced NH_3-SCR of NO_x**
552 In our previous studies, we investigated thermal catalytic NH_3-SCR of NO_x over four
553 catalysts (H-SAPO-34, Mn/SAPO-34, Cu/SAPO-34 and Cu-Mn/SAPO-34). We found that
554 only the Cu/SAPO-34 and Cu-Mn/SAPO-34 catalysts exhibited high NO_x conversion [9]. Our
555 works demonstrated that Cu active sites make a major contribution to the removal of NO_x while
556 doping with Mn forms bimetal active sites, which further enhances the catalytic activities. The
557 NO-TPD profiles of Cu/SAPO-34 and Cu-Mn/SAPO-34 showed a broad peak between 150
558 and 450 ^oC, which can be ascribed to the overlap of two adsorption peaks related to surface
559 nitrite and bridging bidentate nitrates. Compared to Cu/SAPO-34, Mn-doped Cu/SAPO-34
560 enhanced the adsorption of both NO_x and NH_3 [25].
561 In this study, the adsorption of NH_3 on the catalysts remained at a high level, and the
562 formation of NO_2 and nitrates was remarkably increased in the plasma process, especially when
563 adding C_3H_6. Figure 7 shows the proposed reaction pathways of the plasma-enhanced NH_3-
564 SCR of NO_x in the presence of H_2O and C_3H_6 based on the discussions in previous sections.
565 When plasma was used, O atoms produced from the electron impact dissociation of O_2 can
566 react with H_2O to produce OH radicals. It is worth noting that long life active species, such as
567 H_2O_2 and O_3 were not included in the reaction pathway since they would quickly decompose
568 into active species with short lifetimes (e.g. OH and O) due to the relatively high reaction

569 temperature (≥100 ^{o}C) in this study. This argument is supported by the evidence that no O_3 was
570 detected at the outlet of the DBD reactor throughout the experiments, and also the performance
571 of the plasma conversion of NO (without catalyst) was almost independent of the reaction
572 temperature.

573 The formed oxidative species (O and OH) can oxidize NO and C_3H_6 into intermediate
574 products, such as gaseous NO_2, HNO_2, HNO_3 and $C_xH_yO_z$. Unlike the thermal catalytic NH_3-
575 SCR of NO, which is mainly driven by the reactions between NO_2 (ads) and NH_4^+ (L-H
576 mechanism), and NO and coordinated NH_3 (E-R mechanism) [25], in the post-plasma catalytic
577 SCR reaction, the intermediates formed in the plasma process play an important in the
578 subsequent SCR reactions on the catalyst surface. The formed gaseous NO_2 in the NTP creates
579 additional reaction pathways (E-R mechanism) through its reaction with adsorbed NH_4^+ and
580 coordinated NH_3 on the catalyst surface to produce N_2. HNO_3 and HNO_2 in the gas phase can
581 easily react with NH_3 to produce NH_4NO_3 and NH_4NO_2, both of which are known as important
582 intermediates in contributing to the rapid reduction of NO to N_2 on the catalyst surface. The
583 addition of C_3H_6 in the reaction not only enhances the formation of NO_2 in the gas phase by
584 quenching the excess O atoms to limit the reverse reaction (Eq. (5)), but also produces
585 oxygenates which could react with NO on the catalyst surface to produce N_2. Thus, the use of
586 NTP could enhance the NH_3-SCR of NO.

587

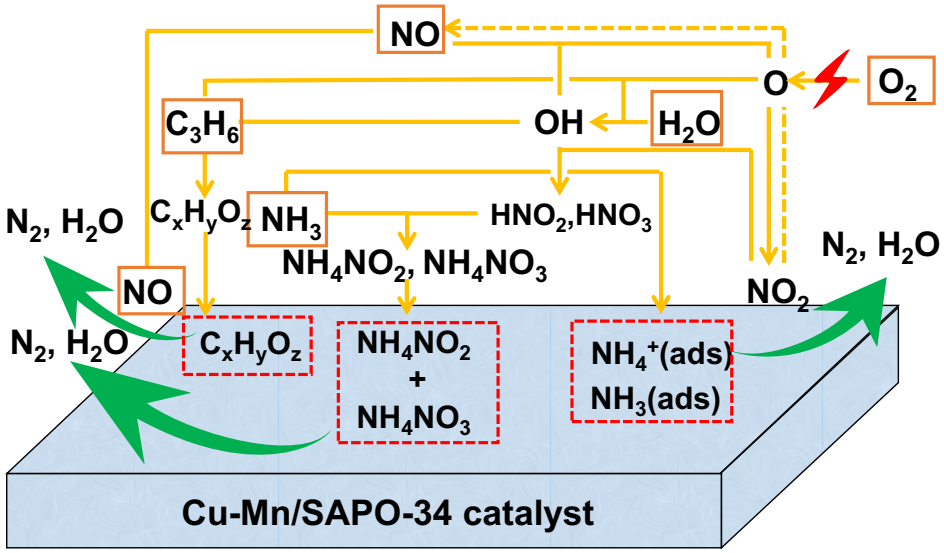

Figure 7. Reaction mechanism of plasma-enhanced NH_3-SCR of NO_x on Cu-Mn/SAPO-34

5. Conclusion

In this study, we have successfully demonstrated that the coupling of a DBD plasma with the Cu-Mn/SAPO-34 catalyst in the PPC configuration is effective for the NH_3-SCR of NO_x at low temperatures (200 ^oC) and oxygen-rich (14 vol.%) conditions. An 80% NO removal and 100% N_2 selectivity can be achieved at a low SEI in the proposed process without NH_3 slip or by-products. The effect of the plasma in the NH_3-SCR of NO_x is more significant at a lower temperature. Unlike the conventional thermal-catalytic process, plasma-assisted NH_3-SCR of NO_x was not affected by the presence of water vapor (5.7 vol.%), while the presence of C_3H_6 enhanced the removal of NO_x. The beneficial effect of the plasma in the NH_3-SCR of NO_x process can be explained as: the formation of NO_2, HNO_2, HNO_3 and oxygenates via the partial oxidation of NO by NTP in the first stage gaseous phase plasma processing enhances the subsequent E-R reaction on the surfaces of the Cu-Mn/SAPO-34 catalyst in the second stage SCR reaction. This work has provided a cost-effective and low-temperature solution for the

development of an NTP-assisted NH_3-SCR process for the removal of NO_x from light-duty diesel engines as well as heavy-duty diesel engines during their cold-start period.

Acknowledgement

The work was financially supported by the National Natural Science Foundation of China (No. 11775189 and U1709209), National Key Research and Development Plan (No. 2018YFB0605200), Natural Science Foundation of Zhejiang Province (NO. LY19B070002), Public Welfare Research Projects of Zhejiang Province (No. 2016C33015), and the Science and Technology Innovation Program of College Students at Zhejiang Province (No. 1260KZN0218063G and No. 1260KZN0218061G). Y. Wang and X. Tu acknowledge the funding from European Union's Horizon 2020 research and innovation programme under the Marie Sklodowska-Curie grant agreement No. 722346. The authors are also grateful to Instrumental Analysis Center of Zhejiang Gongshang University for their technical support.

References

[1] S. C. Anenberg, J. Miller, R. Minjares, L. Du, D. K. Henze, F. Lacey, C. S. Malley, L. Emberson, V. Franco, Z. Klimont, Impacts and mitigation of excess diesel-related NOx emissions in 11 major vehicle markets, Nature, 545 (2017) 467-471.

[2] Q. Wang, J. H. Sohn, J. S. Chung, Thermally stable $Pt/K_2Ti_2O_5$ as high-temperature NOx storage and reduction catalyst. Appl. Catal. B: Environ, 89 (2009) 97—103.

[3] X. Wang, X. Du, S. Liu, G. Yang, Y. Chen, L. Zhang, X. Tu, Understanding the deposition and reaction mechanism of ammonium bisulfate on a vanadia SCR catalyst: A combined DFT and experimental study, Appl. Catal. B: Environ. 260 (2020) 118168.

[4] R. Qu, X. Gao, K. Cen, J. Li, Relationship between structure and performance of a novel cerium-niobium binary oxide catalyst for selective catalytic reduction of NO with NH_3, Appl. Catal. B: Environ. 142-143 (2013) 290-297.

[5] R. Yu, Z. Zhao, S. Huang, W. Zhang, Cu-SSZ-13 zeolite-metal oxide hybrid catalysts with enhanced SO_2-tolerance in the NH_3-SCR of NO_x, Appl. Catal. B: Environ. 269 (2020) 118825.

[6] Y. Shan, J. Du, Y. Yu, W. Shan, X. Shi, H. He, Precise control of post-treatment significantly increases hydrothermal stability of in-situ synthesized cu-zeolites for NH_3-SCR reaction, Appl. Catal. B: Environ. 266 (2020) 118655.

[7] S. Prodinger, M. A. Derewinski, Y. Wang, N. M. Washton, E. D. Walter, J. Szanyi, F. Gao, Y. Wang, C.H.F. Peden, Sub-micron Cu/SSZ-13: Synthesis and application as selective catalytic reduction (SCR) catalysts, Appl. Catal. B: Environ. 201 (2017) 461-469.

[8] S. Ming, Z. Chen, C. Fan, L. Pang, W. Guo, K.B. Albert, P. Liu, T. Li, The effect of copper loading and silicon content on catalytic activity and hydrothermal stability of Cu-SAPO-18 catalyst for NH_3-SCR, Appl. Catal. A: Gen. 559 (2018) 47-56.

[9] L. Huang, X. Wang, S. Yao, B. Jiang, X. Chen, X. Wang, Cu-Mn bimetal ion-

exchanged SAPO-34 as an active SCR catalyst for removal of NOx from diesel engine exhausts, Catal. Comm. 81 (2016) 54-57.

[10] S. Yao, H. Zhang, X. Shen, J. Han, Z. Wu, X. Tang, H. Lu, B. Jiang, T. Nozaki, X. Zhang, A novel four-way plasma-catalytic approach for the after-treatment of diesel engine exhausts, Ind. Eng. Chem. Res. 57 (2018) 1159-1168.

[11] Y. Wang, Z. Liao, S. Mathieu, F. Bin, X. Tu, Prediction and evaluation of plasma arc reforming of naphthalene using a hybrid machine learning mode, J. Hazard. Mater. 404 (2021) 123965.

[12] J. C. Whitehead, Plasma-catalysis: the known knowns, the known unknowns and the unknown unknowns, J. Phys. D: Appl. Phys. 49 (2016) 243001.

[13] H. H. Kim, Y. Teromoto, A. Ogata, H. Takagi, T. Nanba, Plasma catalysis for environmental treatment and energy applications, Plasma Chem. Plasma Process. 36 (2016) 45-72.

[14] A. Bogaerts, X. Tu, J. C. Whitehead, G. Centi, L. Lefferts, O. Guaitella, F. Azzolina-Jury, H. H. Kim, A. B. Murphy, W. F. Schneider, T. Nozaki, J. C. Hicks, A. Rousseau, F. Thevenet, A. Khacef, M. Carreon, The 2020 plasma catalysis roadmap, J. Phys. D: Appl. Phys. 53 (2020) 443001.

[15] T. Wang, X. Zhang, J. Liu, H. Liu, Y. Wang, B. Sun, Effects of temperature on NO_x removal with Mn-Cu/ZSM5 catalysts assisted by plasma, Appl. Therm. Eng. 130 (2018) 1224-1232.

[16] Y. Takahara, A. Ikeda, M. Nagata, Y. Sekine, Low-temperature NO decomposition in

667 humidified condition using plasma-catalyst system, Catal. Today. 211 (2013) 44-52.
668 [17] H. Miessner, K.-P. Francke, R. Rudolph, Plasma-enhanced HC-SCR of NOx in the
669 presence of excess oxygen, Appl. Catal. B: Environ. 36 (2002) 53-62.
670 [18] B. Guan, H. Lin, Q. Cheng, Z. Huang, Removal of NO_x with selective catalytic
671 reduction based on nonthermal plasma preoxidation, Ind. Eng. Chem. Res. 50 (2011)
672 5401-5413.
673 [19] S. Bröer, T. Hammer, Selective catalytic reduction of nitrogen oxides by combining a
674 non-thermal plasma and a V_2O_5-WO_3/TiO_2 catalyst, Appl. Catal. B: Environ. 28
675 (2000) 101-111.
676 [20] B. Ashford, Y. Wang, C. K. Poh, L. Chen, X. Tu, Plasma-catalytic conversion of CO_2
677 to CO over binary metal oxide catalysts at low temperatures, Appl. Catal. B: Environ.
678 276 (2020) 119110.
679 [21] Y. Wang, M. Craven, X. Yu, J. Ding, P. Bryant, J. Huang, X. Tu, Plasma-enhanced
680 catalytic synthesis of ammonia over a Ni/Al_2O_3 catalyst at near-room temperature:
681 Insights into the importance of the catalyst surface on the reaction mechanism. ACS
682 Catal. 9 (2019) 10780-10793.
683 [22] P. Chawdhury, Y. Wang, D. Ray, S. Mathieu, N. Wang, J. Harding, F. Bin, X. Tu, C.
684 Subrahmanyam, A promising plasma-catalytic approach towards single-step methane
685 conversion to oxygenates at room temperature, Appl. Catal. B: Environ. 2021
686 doi.org/10.1016/j.apcatb.2020.119735
687 [23] W. Xu, N. Wang, Y. Chen, J. Chen, X. Xu, L. Yu, L. Chen, J. Wu, M. Fu, A. Zhu, In

688 situ FT-IR study and evaluation of toluene abatement in different plasma catalytic
689 systems over metal oxides loaded γ-Al_2O_3, Catal. Comm. 84 (2016) 61-66.
690 [24] C. E. Stere, J. A. Anderson, S. Chansai, H. Daly, J. J. Delgado, A. Goguet, W. G.
691 Graham, C. Hardacre, S. F. R. Taylor, X. Tu, Z. Wang, H. Yang, Non-thermal plasma
692 activation of gold based catalysts for low temperature water gas shift, Angew. Chem.
693 Int. Ed. 56 (2017) 5579-5583.
694 [25] M. Cheng, B. Jiang, S. Yao, J. Han, S. Zhao, X. Tang, J. Zhang, T. Wang, Mechanism
695 of NH_3 Selective catalytic reduction reaction for NO_x removal from diesel engine
696 exhaust and hydrothermal stability of Cu-Mn/Zeolite catalysts, J. Phys. Chem. C. 122
697 (2018) 455-464.
698 [26] C.E. Stere, W. Adress, R. Burch, S. Chansai, A. Goguet, W.G. Graham, C. Hardacre,
699 Probing a non-thermal plasma activated heterogeneously catalyzed reaction using in
700 situ DRIFTS-MS, ACS Catal. 5 (2015) 956-964.
701 [27] J. Li, W.H. Goh, X. Yang, R.T. Yang, Non-thermal plasma-assisted catalytic NO_x
702 storage over Pt/Ba/Al_2O_3 at low temperatures, Appl. Catal. B Environ. 90 (2009) 360-
703 367.
704 [28] X. Zhang, B.J. Lee, H.G. Im, M.S. Cha, Ozone production with dielectric barrier
705 discharge: Effects of power source and humidity, IEEE Trans. Plasma Sci. 44 (2016)
706 2288-2296.
707 [29] Z. Wu, W. Zhou, X. Hao, X. Zhang, Plasma reforming of n-pentane as a simulated
708 gasoline to hydrogen and cleaner carbon-based fuels, Energy 189 (2019) 116265.

709 [30] S. Zhao, L. Huang, B. Jiang, M. Cheng, J. Zhang, Y. Hu, Stability of Cu-Mn bimetal
710 catalysts based on different zeolites for NOx removal from diesel engine exhaust,
711 Chinese J. Catal. 39 (2018) 800-809
712 [31] Z. Huang, Z. Zhu, Z. Liu, Combined effect of H_2O and SO_2 on V_2O_5/AC catalysts for
713 NO reduction with ammonia at lower temperatures, Appl. Catal. B Environ. 39 (2002)
714 361-368.
715 [32] Z. Lei, B. Han, K. Yang, B. Chen, Influence of H_2O on the low-temperature NH_3-
716 SCR of NO over V_2O_5/AC catalyst: An experimental and modeling study, Chem. Eng.
717 J. 215 (2013) 651-657.
718 [33] S. Yao, X. Shen, X. Zhang, J. Han, Z. Wu, X. Tang, H. Lu, B. Jiang, Sustainable
719 removal of particulate matter from diesel engine exhaust at low temperature using a
720 plasma-catalytic method, Chem. Eng. J. 327 (2017) 343-350.
721 [34] C.-K. Seo, B. Choi, H. Kim, C.-H. Lee, C.-B. Lee, Effect of ZrO_2 addition on de-
722 NO_x performance of Cu-ZSM-5 for SCR catalyst, Chem. Eng. J. 191 (2012) 331-340.
723 [35] P.G. Blakeman, E.M. Burkholder, H.-Y. Chen, J.E. Collier, J.M. Fedeyko, H. Jobson,
724 R.R. Rajaram, The role of pore size on the thermal stability of zeolite supported Cu
725 SCR catalysts, Catal. Today. 231 (2014) 56-63.
726 [36] S.L. Hill, H.H. Kim, S. Futamura, J.C. Whitehead, The destruction of atmospheric
727 pressure propane and propene using a surface discharge plasma reactor, J. Phys.
728 Chem. A 112 (2008) 3953-2958.
729 [37] R. Dorai, M.J. Kushner, Effect of multiple pulses on the plasma chemistry during the

730 remediation of NOx using dielectric barrier discharges, J. Phys. Appl. Phys. 34 (2001)
731 574-583.
732 [38] Limits and Measurement Methods for Emissions from Light-Duty Vehicles (China
733 V); Ministry of Environment Protection of China, 2013.
734 [39] B. Chen, R. Xu, R. Zhang, N. Liu, Economical way to synthesize SSZ-13 with
735 abundant ion-exchanged Cu+ for an extraordinary performance in selective catalytic
736 reduction (SCR) of NO_x by ammonia, Environ. Sci. Technol. 48 (2014) 13909-13916.
737 [40] C. Niu, X. Shi, F. Liu, K. Liu, L. Xie, Y. You, H. He, High hydrothermal stability of
738 Cu-SAPO-34 catalysts for the NH_3-SCR of NOx, Chem. Eng. J. 294 (2016) 254-263.
739 [41] K. Xie, J. Woo, D. Bernin, A. Kumar, K. Kamasamudram, L. Olsson, Insights into
740 hydrothermal aging of phosphorus-poisoned Cu-SSZ-13 for NH_3-SCR, Appl. Catal. B
741 Environ. 241 (2019) 205-216.
742 [42] S. Yao, S. Weng, Y. Tang, C. Zhao, Z. Wu, X. Zhang, S. Yamamoto, S. Kodama,
743 Characteristics of OH production by O_2/H_2O pulsed dielectric barrier discharge,
744 Vacuum. 126 (2016) 16-23.
745 [43] H. Sjövall, E. Fridell, R.J. Blint, L. Olsson, Identification of adsorbed species on Cu-
746 ZSM-5 under NH_3 SCR conditions, Top. Catal. 42 (2007) 113-117.
747 [44] L. Ma, Y. Cheng, G. Cavataio, R.W. McCabe, L. Fu, J. Li, In situ DRIFTS and
748 temperature-programmed technology study on NH_3-SCR of NO_x over Cu-SSZ-13 and
749 Cu-SAPO-34 catalysts, Appl. Catal. B: Environ. 156 (2014) 428-437.
750 [45] F. Liu, H. He, Structure-activity relationship of iron titanate catalysts in the selective

751 catalytic reduction of NOx with NH_3, J. Phys. Chem. C. 114 (2010) 16929-16936.
752 [46] M.P. Ruggeri, A. Grossale, I. Nova, E. Tronconi, H. Jirglova, Z. Sobalik, FTIR in situ
753 mechanistic study of the NH_3/NO/NO_2 “Fast SCR” reaction over a commercial Fe-
754 ZSM-5 catalyst, Catal. Today. 184 (2012) 107-114.
755 [47] G. Zhou, B. Zhong, W. Wang, X. Guan, B. Huang, D. Ye, H. Wu, In situ DRIFTS
756 study of NO reduction by NH_3 over Fe-Ce-Mn/ZSM-5 catalysts, Catal. Today. 175
757 (2011) 157-163.
758 [48] L. Wang, W. Li, S.J. Schmieg, D. Weng, Role of Brønsted acidity in NH_3 selective
759 catalytic reduction reaction on Cu/SAPO-34 catalysts, J. Catal. 324 (2015) 98-106.
760 [49] K. Góra-Marek, K. Brylewska, K.A. Tarach, M. Rutkowska, M. Jabłońska, M. Choi,
761 L. Chmielarz, IR studies of Fe modified ZSM-5 zeolites of diverse mesopore
762 topologies in the terms of their catalytic performance in NH_3-SCR and NH_3-SCO
763 processes, Appl. Catal. B Environ. 179 (2015) 589-598.
764 [50] D. Wang, L. Zhang, J. Li, K. Kamasamudram, W.S. Epling, NH_3-SCR over
765 Cu/SAPO-34-Zeolite acidity and Cu structure changes as a function of Cu loading,
766 Catal. Today 231 (2014) 64-74.
767 [51] B. Jiang, Z. Li, S. Lee, Mechanism study of the promotional effect of O_2 on low-
768 temperature SCR reaction on Fe-Mn/TiO_2 by DRIFT, Chem. Eng. J. 225 (2013) 52-58.
769 [52] A. Grossale, I. Nova, E. Tronconi, D. Chatterjee, M. Weibel, The chemistry of the
770 NO/NO_2-NH_3 “fast” SCR reaction over Fe-ZSM5 investigated by transient reaction
771 analysis, J. Catal. 256 (2008) 312-322.

[53] K. Leistner, O. Mihai, K. Wijayanti, A. Kumar, K. Kamasamudram, N.W. Currier, A. Yezerets, L. Olsson, Comparison of Cu/BEA, Cu/SSZ-13 and Cu/SAPO-34 for ammonia-SCR reactions, Catal. Today 258 (2015) 49-55.

[54] J.S. Chang, The role of H_2O and NH_3 on the formation of NH_4NO_3 aerosol particles and De-NO_x under the corona discharge treatment of combustion flue gases, J. Aerosol Sci. 20 (1989) 1087-1090.

[55] R.G. Tonkyn, S.E. Barlow, J.W. Hoard, Reduction of NO_x in synthetic diesel exhaust via two-step plasma-catalysis treatment, Appl. Catal. B Environ. 40 (2003) 207-217.

[56] Y. Cai, L. Zhang, J. Wang, Z. W. Zhao, W. Jing, Research on plasma chemistry reactions in $C_3H_6/NO/O_2/N_2$ mixture gases, Plasma Sci. Technol. 12 (2010) 482.

[57] K. Ueda, J. Ohyama, K. Sawabe, A. Satsuma, Structure-activity relationship of iron oxides for NO reduction in the presence of C_3H_6, CO, and O_2, Chem. Eur. J. 25 (2019) 13964-13971.

[58] B. J. Lee, H. Kang, J. O. Jo, Y. S. Mok, Consideration of the role of plasma in a plasma-coupled selective catalytic reduction of nitrogen oxides with a hydrocarbon reducing agent, Catalysts 7 (2017) 325.